# MUC1-ND interacts with TRPV1 to promote corneal epithelial cell proliferation in diabetic dry eye mice by partly activating the AKT signaling pathway

HAIQIONG LI[1,2*], YU ZHANG[1*], YUTING CHEN[1], RONG ZHU[1], WEIKANG ZOU[1], HUI CHEN[1], JIA HU[1], SONGFU FENG[1], YANYAN ZHONG[1] and XIAOHE LU[1]

[1]Department of Ophthalmology, Zhujiang Hospital, Southern Medical University, Guangzhou, Guangdong 510220, P.R. China; [2]School of Laboratory Medicine and Biotechnology, Southern Medical University, Guangzhou, Guangdong 510220, P.R. China

Received May 22, 2024; Accepted August 14, 2024

DOI: 10.3892/mmr.2024.13337

**Abstract.** Although both mucin1 (MUC1) and transient receptor potential cation channel subfamily V member 1 (TRPV1) have been reported to be associated with dry eye (DE) disease, whether they interact and their regulatory roles in diabetic DE disease are unknown. Diabetic DE model mice were generated by streptozotocin induction and assessed by corneal fluorescein staining, tear ferning (TF) tests, phenol red thread tests, hematoxylin and eosin staining of corneal sections and periodic acid Schiff staining of conjunctival sections. Cell proliferation was measured by CCK8 assay. Western blotting was performed to measure protein expression. Primary mouse corneal epithelial cells (MCECs) were cultured after enzymatic digestion. Immunofluorescence staining of MCECs and frozen corneal sections was conducted to assess protein expression and colocalization. Coimmunoprecipitation was performed to detect protein-protein interactions. It was found that, compared with control mice, diabetic DE mice exhibited increased corneal epithelial defects, reduced tear production, poorer TF pattern grades and impaired corneal and conjunctival tissues. *In vivo* and *in vitro* experiments showed that hyperglycemia impaired cell proliferation, accompanied by decreased levels of the MUC1 extracellular domain (MUC1-ND) and TRPV1. Additionally, it was found that capsazepine (a TRPV1 antagonist) inhibited the proliferation of MCECs. Notably, MUC1-ND was shown to interact with the TRPV1 protein in the control group but not in the diabetic DE group. It was also found that the AKT signaling pathway was attenuated in the diabetic DE mice and downstream of TRPV1. MUC1-ND interacted with TRPV1, partly activating the AKT signaling pathway to promote MCEC proliferation. The present study found that the interaction of MUC1-ND with TRPV1 promotes MCEC proliferation by partly activating the AKT signaling pathway, providing new insight into the pathogenesis of corneal epithelial dysfunction in diabetic DE disease.

*Correspondence to:* Dr Yanyan Zhong or Professor Xiaohe Lu, Department of Ophthalmology, Zhujiang Hospital, Southern Medical University, 253 Industrial Avenue, Haizhu, Guangzhou, Guangdong 510220, P.R. China
E-mail: zhongyanyan07@163.com
E-mail: luxiaohe@i.smu.edu.cn

*Contributed equally

*Key words:* N-terminal α subunit of mucin1, transient receptor potential cation channel subfamily V member 1, AKT pathway, proliferation, diabetic dry eye disease

## Introduction

Diabetes mellitus (DM) has become a global public health crisis, affecting 537,000,000 individuals worldwide in 2021 (1) and has been identified as a risk factor for dry eye (DE) disease (2,3). Clinical studies have found that over half of patients with diabetes have DE disease, which progresses as the duration of diabetes increases (4,5). Diabetic DE disease is characterized by decreased corneal sensitivity, reduced tear secretion, altered tear proteins and corneal epithelial lesions (6-9). Hyperglycemia impairs corneal epithelial basal cells and the basement membrane (10), but the specific mechanism by which corneal epithelial lesions form remains unclear. Therefore, understanding the molecular mechanism of corneal epithelial dysfunction in diabetic DE disease is desirable.

Mucin1 (MUC1) is a member of the mucin family, which contains O-glycosylated proteins that play key roles in the tear film homeostasis and protect the ocular surface (11,12). MUC1 is expressed across the cornea and conjunctival epitheliums in humans but only in the corneal epithelium in mice (13,14). The extracellular domain of the N-terminal alpha subunit of MUC1 (MUC1-ND) is responsible for cell adhesion and the cytoplasmic tail of MUC1 (MUC1-CT) is involved in cell signaling (15). Previous studies have reported that the MUC1-CT carries out extensive functions beyond its ability to interact with several proteins, such as Src, catenin β1 (CTNNB1) and ErbBs (16,17). For example, MUC1-CT promotes cell adhesion by binding CTNNB1/β-catenin and junction plakoglobin/γ-catenin. Additionally, MUC1-CT

facilitates RAB27A-mediated exosome secretion by interacting with the pocket of RAB27A (18). Studies have also found that MUC1 is extracellularly cleaved within the sperm protein, enterokinase and agrin (SEA) module in MUC1-ND by ADAM17 or MT1MMP (19,20). Miyazaki *et al* (21) show that MUC1-ND functions as a hydrophilic barrier that hinders the entry of lipophilic anticancer drugs, leading to chemoresistance. Increasing evidence suggests that MUC1 is also implicated in inflammatory diseases (22,23). However, the function of MUC1 and the underlying molecular mechanism involved in diabetic DE disease remain unclear.

Transient receptor potential cation channel subfamily V member 1 (TRPV1), a nociceptive sensor, is associated with ocular surface pain (24). TRPV1 enhances the excitability of nociceptive sensors activated by heat, protons and inflammatory mediators (25). TRPV1 channel dysfunction is shown to induce decreased corneal sensitivity, which is correlated with the pathogenesis of DE disease (6). Notably, TRPV1 is found to be translocated to astrocyte membranes to promote migration and inflammatory infiltration in models of neonatal hypoxic-ischemia and hypoxic hypoglycemia (26,27), but it is involved in the protection of diabetic rats after hypoxic preconditioning (28), suggesting that TRPV1 plays a complex role in the inflammatory process. The TRPV1 channel activation is also shown to induce the proliferation and migration of human corneal epithelial cells (29). MUC1 interacts with TRPV5 through galectin 3, enhancing renal TRPV5 activity and preventing kidney stone formation (30). In addition, MUC1 decreases the internalization of Ca-selective TRP channels TRPV5 and TRPV6 while promoting their presence on the cell surface, aiding in maintaining $Ca^{2+}$ balance (31). These findings highlight the close relationship between MUC1 and TRP channels. However, whether MUC1 interacts with TRPV1 and the underlying signaling mechanism in corneal epithelial cell proliferation remain to be elucidated.

The present study found decreased proliferation of mouse corneal epithelial cells (MCECs), accompanied by decreased levels of MUC1-ND and TRPV1, in diabetic DE mice. In addition, capsazepine (CPZ; a TRPV1 antagonist) restricted the proliferation of MCECs. There was an interaction between MUC1-ND and the TRPV1 protein in the control group but not in the diabetic DE group. Furthermore, the activation of the AKT signaling pathway was attenuated in diabetic DE mice and it was downstream of TRPV1. In summary, the results illustrated that the MUC1-ND/TRPV1/AKT axis plays an essential role in the proliferation of MCECs and provided new insight into the pathogenesis of corneal epithelial dysfunction in diabetic DE disease.

## Materials and methods

*Reagents*. Primary antibodies against the following were provided by Abcam: MUC1-ND (cat. no. ab45167), AKT1/2/3 (cat. no. ab185633), p-AKT (Thr308; cat. no. ab38449), Bcl2 (cat. no. ab182858), β-Actin (cat. no. ab8227) and β-tubulin (cat. no. ab6046). Primary antibodies against the following were purchased from Proteintech Group, Inc.: MUC1-CT (cat. no. 23614-1-AP), TRPV1 (cat. no. 66983-1-Ig) and phosphorylated (p-)AKT (Ser473; cat. no. 28731-1-AP). Primary antibodies against the following were purchased from Cell Signaling Technology, Inc.: Caspase3 (cat. no. 9662) and IgG (cat. no. 2729). The primary antibodies of CK3+12 (cat. no. Bs-2369R) and TRPV1 (cat. no. Bs-23926R) were purchased from BIOSS. The following secondary antibodies were obtained from Invitrogen (Thermo Fisher Scientific, Inc.): Alexa Fluro 488 (goat anti-mouse, cat. no. a11029; goat anti-rabbit, cat. no. a11008) and Alexa Fluro 594 (goat anti-mouse, cat. no. a11032; goat anti-rabbit, cat. no. a11012). The following secondary antibodies were obtained from Abcam: goat anti-rabbit IgG/HRP (cat. no. ab6721) and goat anti-mouse IgG/HRP (cat. no. ab6789). CPZ (cat. no. HY15640) and MK2206 (cat. no. HY-10358) were purchased from MedChemExpress.

*Animals*. Male C57BL/6 mice at aged of 6-8-weeks and weighing 18-22 g were purchased from the Experimental Animal Center of Southern Medical University (Guangzhou, China). Mice were cared for in accordance with the ARVO Statement for the Use of Animals in Ophthalmic and Vision Research (32). All experimental procedures received approval from the Institutional Animal Care and Use Committee of Southern Medical University (Guangzhou, China; approval no. LAEC-2021-032). The mice were housed in a specific pathogen-free rated animal vivarium (temperature, 20-26˚C; light/dark cycle, 12/12 h; humidity: 40-70%) and the research team monitored the animals twice daily. Health assessments included monitoring weight (twice weekly), food and water intake and a general evaluation of activity levels, panting and fur condition. A total of 155 mice were used, of which 149 were euthanized using carbon dioxide ($CO_2$) inhalation. The absence of a heartbeat and dilation of pupils for a period of ≥5 min were verified in order to confirm mortality; if these conditions were not met, cervical dislocation was then performed. Sacrificed mice were used for corneal and conjunctival histopathology, as well as for the primary culture of mouse corneal epithelial cells. Of the diabetic group, six succumbed unexpectedly, probably due to complications associated with diabetes. The duration of the experiment ranged from 1.5-2.5 months. The ocular surface parameter measurements were conducted in a non-invasive and painless manner. Additionally, 3% sodium pentobarbital was administered intraperitoneally at a dose of 50 mg/kg to induce sedation in the mice.

*Diabetic DE mouse model*. A streptozotocin (STZ; MilliporeSigma)-induced diabetic mouse model was established and Na-citrate buffer administered to the control group. To induce DM, mice were fasted for 4 h and injected with a low dose of STZ (50 mg/kg) for 5 consecutive days. Mice were fed a normal diet (control group) or a high-fat/high-sugar diet (DM group). Corneal fluorescein staining (CFS), tear ferning (TF) tests and phenol red thread tests were performed before treatment and 7, 30 and 60 days after the final injection. Corneal sections were conducted hematoxylin and eosin (H&E) staining on days 30 and 60 after the final injection and conjunctival sections were stained with periodic acid Schiff (PAS) on days 30 and 60 after the final injection. After the aforementioned evaluation, a diabetic DE mouse model was established and the mice were divided into a control group and a diabetic DE group.

*CFS*. To estimate the defects of corneal epithelium in the mice, 1 $\mu$l of 1% liquid sodium fluorescein was dropped into the lateral conjunctival sac. After 3 min, the eyes were imaged with a slit-lamp microscope (SL-17; Kowa Optimed, Inc.) under cobalt blue light. A total of four quadrants of cornea were scored by two independent blinded individuals using a standardized four-scale system: 0 points for no staining; 1 point for <30 stained dots; 2 points for >30 non-diffuse stained dots; 3 points for severe diffuse staining but no positive plaques; and 4 points for positive fluorescein plaques. The total score was the sum of four quadrants scores (0-16).

*TF tests*. Tear samples (0.5 $\mu$l) collected from each eye of the mice were dried on a microscopic glass slide at room temperature and <40% humidity for 20 min. The TF patterns were imaged under a Leica bright field microscope (Leica Microsystems GmbH; magnification, x10) and analyzed using a new 5-point grading scale (33) from 0 to 4; a grade higher than grade 2 indicated possible DE disease.

*Tear production*. The amount of tears was quantified by the phenol red thread (Zone-Quick; Showa Yakuhin Kako Co., Ltd.). A smooth tweezer placed the folded end of the thread into the temporal one-third of the lateral conjunctival sac for 15 sec. After 15 sec, the wetting length of thread (red portion) was measured in millimeters.

*Histopathology*. The eyeball and eyelid tissues of the mice were excised and fixed in 4% paraformaldehyde (PFA) at 4˚C overnight. The tissues were dehydrated using varying concentrations of ethanol, followed by transparency treatment with xylene, immersion in wax, and embedding in paraffin. Paraffin sections were cut into 4 $\mu$m sagittal sections with a microtome (RM2245; Leica Microsystems GmbH). Frozen sections were sliced into sagittal sections (6-10 $\mu$m thick) with a microtome (CM1950; Leica Microsystems GmbH). H&E or PAS were performed on the paraffin sections, while the frozen sections underwent immunofluorescence (IF) staining.

To evaluate defects in the corneal epithelium, eye sections were stained with hematoxylin for 5 min and eosin for 1 min at room temperature. To evaluate the goblet cell density of the conjunctiva, PAS staining of the conjunctiva sections was performed using a PAS kit (Beijing Solarbio Science & Technology Co., Ltd.). The eye sections were stained with periodic acid for 5 min and Schiff for 10 min at room temperature. Images of the staining sections were captured under a microscope (DM2500; Leica Microsystems GmbH). The thickness of the corneal epithelium in captured images was measured with ImageJ 1.8 (National Institutes of Health). The goblet cells in the superior and inferior conjunctiva were counted by two independent blinded individuals in three sections of each eye. The average number of the three sections was recorded as the goblet cell density of the eye.

*Isolation and culture of primary mouse corneal epithelial cells (MCECs)*. MCECs were isolated by enzymatic digestion. The mice from the control group and diabetic DE group were sacrificed by $CO_2$. Animals were placed into $CO_2$ anesthesia box with ≥7.5% $CO_2$ and after the animals gradually lost consciousness, the $CO_2$ concentration was raised to 100% until respiratory cardiac arrest occurred. Their eyes were surgically extracted, placed into a 10 cm dish (Corning Life Sciences) and washed with PBS three times. Under a Leica S9 stereomicroscope (Leica Microsystems GmbH), the lens and posterior eyecups were discarded to detach the corneas, which were dissected into four equal pieces. Afterward, the corneas were transferred into a new 10 cm dish containing 0.25% EDTA-trypsin (Gibco; Thermo Fisher Scientific, Inc.) and digested at 37˚C for 10 min. The control group cells were maintained in DMEM/F12 (Gibco; Thermo Fisher Scientific, Inc.) containing 10% FBS, 1% nonessential amino acids (Gibco; Thermo Fisher Scientific, Inc.), insulin (5 $\mu$g/ml; MilliporeSigma) and 100 U/ml penicillin/streptomycin (Gibco; Thermo Fisher Scientific, Inc.). The diabetic DE group cells were cultured in DMEM with high glucose and the same supplements used to maintain the control group.

*CCK8 assay*. Cell Counting Kit-8 (CCK8; Gibco; Thermo Fisher Scientific, Inc.) solution was used to detect the cell proliferative capacity of each group or treated cells. Primary MCECs from each group were cultured at 2,000 cells per well in 96-well plates (Corning Life Sciences) for 3 days. CCK8 solution (10 $\mu$l) was added to each well at 4, 24, 48 and 72 h and then incubated at 37˚C under 5% $CO_2$ for 2 h. The optical density (OD) was measured at 450 nm wavelength via a microplate reader (BioTek; Agilent Technologies, Inc.) and the cell growth curves were plotted.

To evaluate the effect of CPZ or MK2206 on cell viability, primary MCECs from each group were treated with DMSO-soluble CPZ (0, 10, 30 $\mu$M) or water-soluble MK2206 (1 $\mu$M) for 24 h. After the addition of CCK8 solution and incubation for 1.5 h, the OD was measured and the cell viability was calculated.

*Cell IF staining*. Primary MCECs were stained with cytokeratin 3+12 (CK3+12) for cell identification. The primary MCECs were cultured on 6-well plates (Corning Life Sciences) with round cover slips (12 mm) for 24 h. Then, the cells were first fixed in 4% PFA for 15 min at room temperature and blocked with 5% BSA (Thermo Fisher Scientific, Inc.) in PBS. Following incubation with the primary antibodies anti-CK3+12 (1:200), anti-MUC1-CT (1:200) and anti-TRPV1 (1:200) and fluorescent secondary antibodies (1:500), the cells were counterstained with DAPI for 5 min at room temperature (cat. no. ab285390; Abcam). Images were captured with an inverted confocal microscope (Nikon Corporation).

*IF colocalization analysis*. Frozen corneal sections were fixed in cold acetone for 10 min at 4˚C. After blocking with 5% BSA in PBS for 1 h at room temperature, they were incubated with anti-MUC1-ND (1:200) and anti-TRPV1 (1:300) overnight at 4˚C and stained with secondary antibodies (1:500) for 1 h at room temperature, then counterstained with DAPI for 5 min at room temperature. Images were captured with a Nikon Ti-E microscope (Nikon Corporation) equipped with an A1R confocal system. IF colocalization analysis was conducted with ImageJ 1.8 (National Institutes of Health).

*Western blotting*. Primary MCECs from each group or treated cells were lysed in RIPA (Thermo Fisher Scientific, Inc.) lysis

Table I. Blood glucose, weight and food intake of mice before and after treatment.

| Group | | Control | Diabetes mellitus |
|---|---|---|---|
| Blood glucose (mmol/l) | Baseline | 6.24±0.78 | 5.18±0.57 |
| | 7 days | 6.80±0.84 | 24.83±1.94[a] |
| | 30 days | 7.72±0.62 | 25.49±1.83[a] |
| Body weight (g) | Baseline | 20.18±0.64 | 20.35±0.71 |
| | 7 days | 21.28±0.64 | 21.81±0.78 |
| | 30 days | 26.96±0.81 | 23.61±1.08[a] |
| Food intake (g/day) | Baseline | 4.70±0.43 | 5.05±0.50 |
| | 7 days | 5.55±0.71 | 8.75±0.58[a] |
| | 30 days | 6.16±0.58 | 8.83±0.46[a] |

The data are expressed as means and standard deviation (n=10). [a]P<0.001.

buffer mixed with 1% phosphate inhibitor cocktail 100X (Gibco; Thermo Fisher Scientific, Inc.) and 1% protease inhibitor cocktail 100X (Gibco; Thermo Fisher Scientific, Inc.). A BCA protein assay kit (Nanjing KeyGen Biotech Co., Ltd.) was used to examine the protein concentration. Equal amounts of protein samples were loaded to sodium dodecyl sulfate-polyacrylamide gel electrophoresis (SDS-PAGE) and moved to polyvinylidene fluoride membranes (MilliporeSigma). A total of 30 $\mu$g protein/lane was loaded, and 5% stacking gel and 8, 10 and 12% separating gel was used. The membranes were blocked with 5% BSA for 2 h at room temperature and incubated with primary antibodies against the following overnight at 4˚C: p-AKT (Ser473) (1:1,000), MUC1-CT (1:800), MUC1-ND (1:1,000), TRPV1 (1:1,000), AKT1/2/3 (1:1,500), p-AKT (Thr308) (1:800), Bcl2 (1:2,000), caspase3 (1:1,000) and β-Actin (1:1,000). After incubation with secondary antibodies (1:2,000) for 1 h, the bands were detected by an enhanced chemiluminescence (ECL) system (Bio-Rad ChemiDoc XRS+; Bio-Rad Laboratories, Inc.). Quantification of the band intensity was conducted with ImageJ 1.8 (National Institutes of Health).

*Co-immunoprecipitation (Co-IP) assays*. Co-IP assays were performed by using a Pierce cross-linked bead immunoprecipitation/coprecipitation kit (cat. no. 88805; Thermo Fisher Scientific, Inc.). First, primary MCECs were lysed with IP lysis buffer and centrifuged at 10,000 x g for 10 min at 4˚C. Then, the lysates with 500 $\mu$g proteins were immunoprecipitated with 5 $\mu$g anti-TRPV1 (1:20), 5 $\mu$g anti-MUC1-ND (1:20) or 1 $\mu$g IgG (1:50) coupled to protein A/G magnetic beads at room temperature for 1.5 h. The beads were washed in IP buffer and eluted in IP elution buffer for 10 min. All incubations were taken on a rotator or mixer. The beads were washed to remove unbound proteins, and a low pH elution buffer was used to separate bound antigen from the antibody cross-linked beads. Neutralization buffer was included to prevent precipitation of the isolated antigen and to ensure protein activity in downstream applications. Western blotting was conducted to detect the bound proteins.

*Statistical analysis*. All data are shown as the mean ± standard deviation. Statistical tests were performed by SPSS 20.0 (IBM Corp.) software and graphs were prepared by Prism 8.0 (GraphPad; Dotmatics) software. Student's t-test was used to compare differences of two groups. Comparisons between more than two groups were made by one-way ANOVA followed by the LSD test or Welch test with Dunn's multiple-comparisons test. P<0.05 was considered to indicate a statistically significant difference.

## Results

*Establishment of a diabetic DE mouse model*. To establish a diabetic DE mouse model, STZ-induced diabetic mice were created on a high-fat and high-sugar diet and phenol red thread tests, CFS, TF tests and histological examinations were conducted to evaluate DE disease.

First, STZ was used to induce diabetes in mice and the mice were then followed for 60 days following the final STZ injection to determine changes in the ocular surface as the duration of diabetes increased (Fig. 1A). Mice in the DM group were confirmed to have higher blood glucose levels, lower body weights and increased food intake compared with those of mice in the control group (Table I), indicating that the diabetic mice had been successfully created. In addition, the mice were observed at baseline and 7, 30 and 60 days following treatment by phenol red thread, CFS and TF tests (Fig. 1B). As illustrated in Fig. 1C, the tear production was similar level between the control and DM groups at baseline and on days 7 after treatment. However, the diabetic mice exhibited decreased tear production on days 30 and 60 after STZ injection. These results demonstrated that the lacrimal gland function in secreting tear fluids was impaired in the DM group on days 30 and 60 after STZ injection.

CFS (Fig. 1D) of the DM group after STZ injection showed scattered punctate staining on days 7, severe diffuse staining on days 30 and positive fluorescein plaque staining on days 60. However, no staining of the corneas of the control group was observed. The DM group mice had a higher CFS score than the control group mice (Fig. 1E). After treatment, corneal epithelial defects in the diabetic mice increased on days 30 and days 60 following STZ injection.

The diabetic mice exhibited decreased TF and poor TF pattern grades on days 7, 30 and 60 after treatment

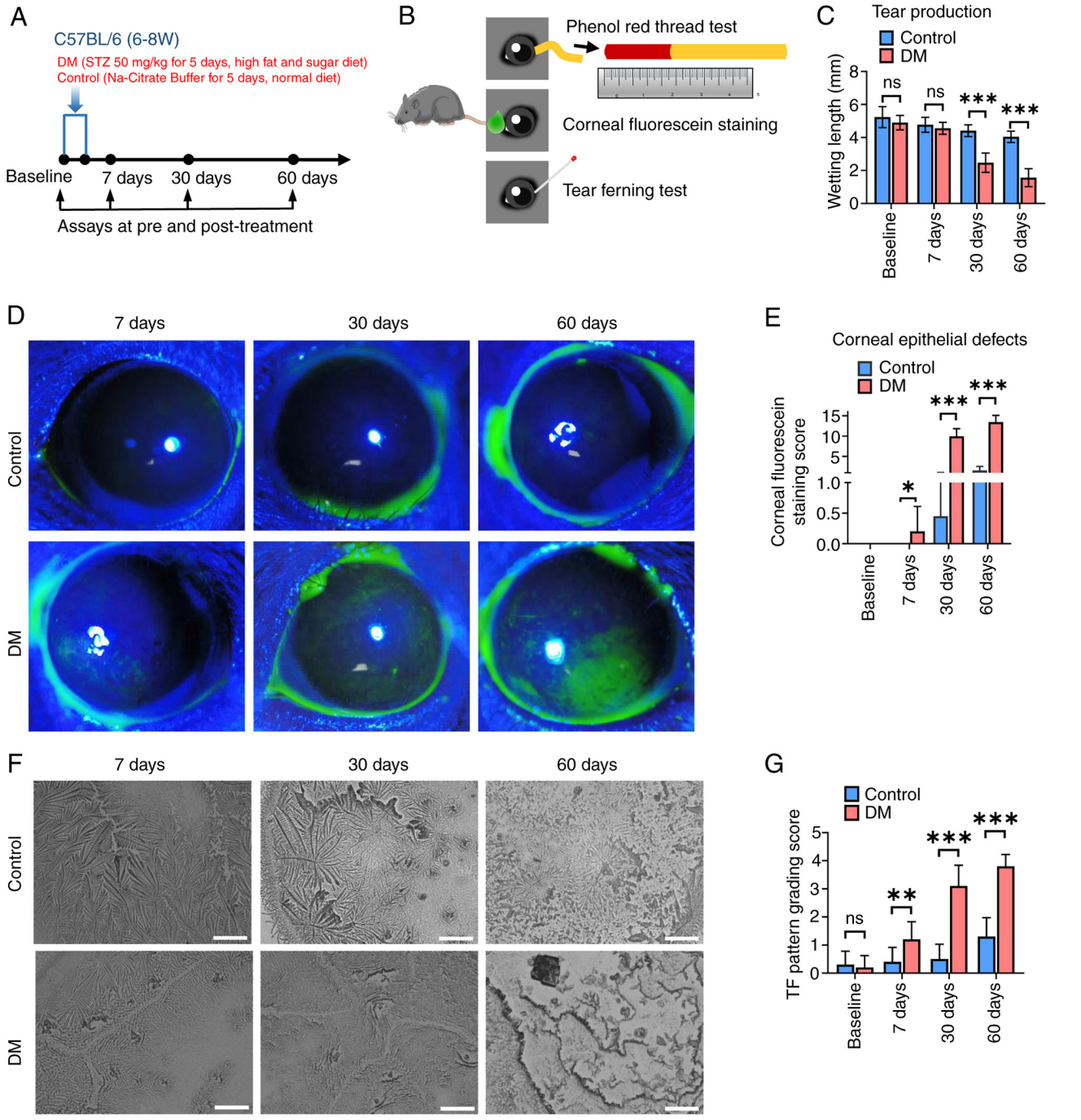


Figure 1. STZ-induced diabetic mice and evaluation of DE disease. (A and B) Experimental protocol for diabetic mice preparation and assays to evaluate DE disease at various time points. (C) Quantitative analysis of tear production using the phenol red thread test. (D) CFS was imaged by a slit-lamp microscope under cobalt blue light on days 7, 30 and 60 after final injection. Green-stained areas represent corneal epithelial defects. (E) Quantitative analysis of corneal epithelial damage. (F) Representative images captured during the TF test at baseline and days 7, 30 and 60 after final injection. Scale bar, 100 $\mu$m. (G) Quantitative analysis of TF pattern grades. In C, E and G, the mean values ± standard deviation are shown (n=20 eyes, 10 animals per group). A two-sided Student's t test was used to calculate the statistical significance. ns, not significant, $^{*}$P<0.05, $^{**}$P<0.01, $^{***}$P<0.001. STZ, streptozotocin; DE, dry eye; CFS, corneal fluorescein staining; TF, tear ferning.

(Fig. 1F and G). At baseline, there was no significant difference between the two groups. On 7, 30 and 60 days after treatment, the TF grade of the DM group was significantly higher than that of the control group. These findings suggested that in the diabetic mice, the composition and proportions of tear proteins, especially mucins, were already changed.

Furthermore, histopathologic examination of the cornea and conjunctiva were performed. During the 60-day follow-up, it was found that compared with the control mice, the diabetic mice exhibited a thinner corneal epithelium with reduced cell layers and the disturbance of basal cells (Fig. 2A). The thickness of the corneal epithelium in H&E-stained sections (Fig. 2B) was significantly smaller in the DM group compared with the control group on days 30 and 60 (P<0.01, P<0.01), suggesting that DM had injured the corneal epithelium. As shown in Fig. 2C and D, the diabetic mice had a lower goblet

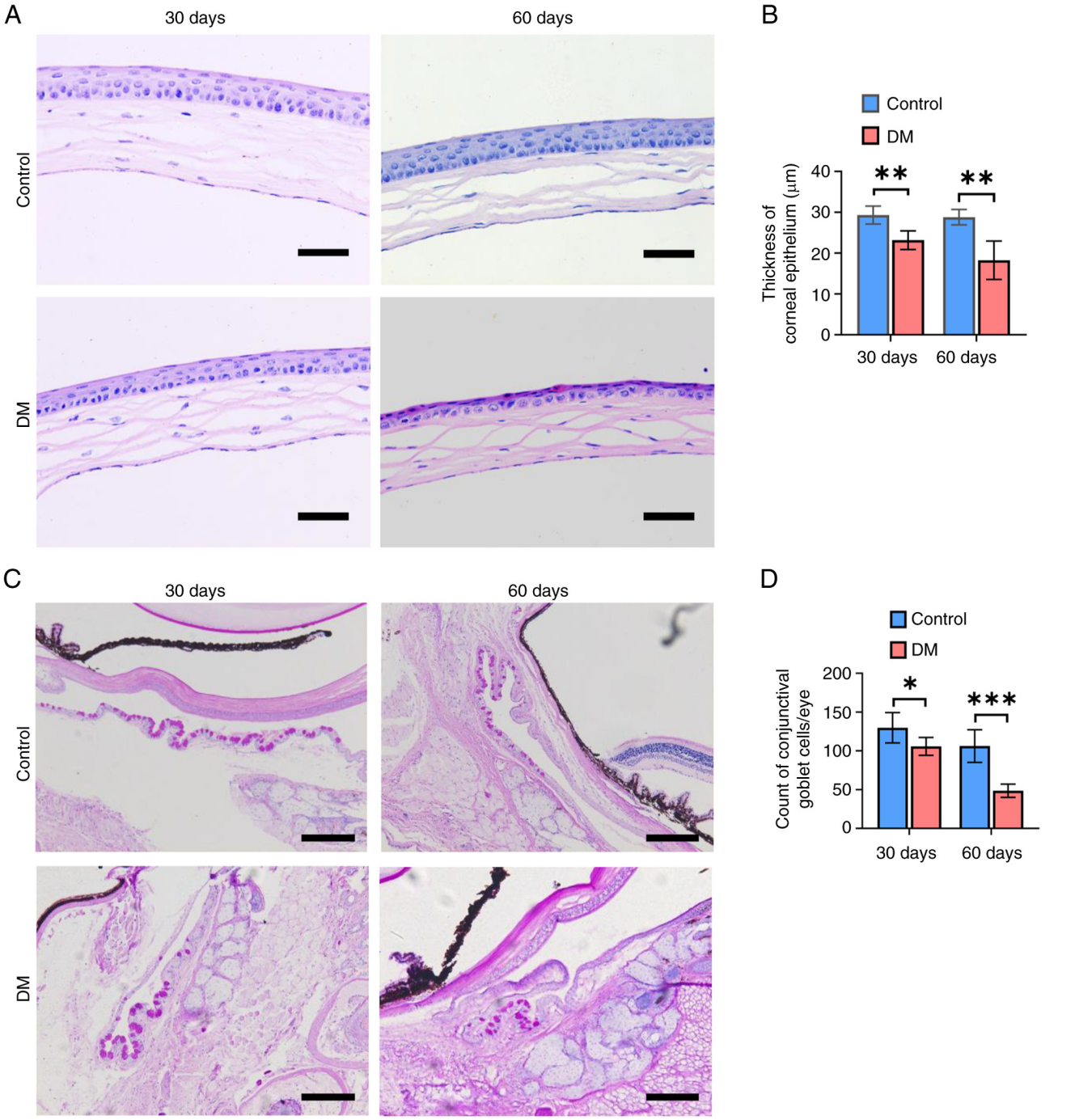


Figure 2. Histopathology of the ocular surface tissues. (A) Representative images of corneal sections following hematoxylin and eosin staining. Scale bar, 50 $\mu$m. (B) Statistical analysis of the thickness of the corneal epithelium, as measured in images of (A). (C) Representative images of conjunctival sections stained with PAS. Scale bar, 200 $\mu$m. (D) The goblet cell density in PAS-stained sections. In (B) and (D), data are show as mean ± standard deviation (n=5 animals per group). A two-tailed Student's t-test was used to calculate the statistical significance. ns, not significant, $^{*}$P<0.05, $^{**}$P<0.01, $^{***}$P<0.001. PAS, periodic acid Schiff; DM, diabetes mellitus.

cell density than the control mice on days 30 and days 60 after treatment, illustrating that DM had impaired the number and function of conjunctival goblet cells.

After the aforementioned evaluation, a diabetic DE mouse model was established. Taken together, the results indicated that the diabetic mice exhibited decreased tear secretion, increased corneal epithelial damage and poorer TF grades, accompanied by corneal epithelium and conjunctiva injury, proving that the diabetic DE mouse model had been created.

*Isolation, culture and identification of primary MCECs.* To explore the mechanism of corneal epithelial lesions in the diabetic DE mice *in vitro*, primary corneal epithelial cells were cultured. The corneas of mice in the control and diabetic DE groups were isolated and primary MCECs from the two groups by cultured enzymatic digestion (Fig. 3A). The morphology of primary MCECs in the two groups cultured on day 10 is shown in Fig. 3B. The MCECs grew by static adherence and the cells in the two groups had similar shapes

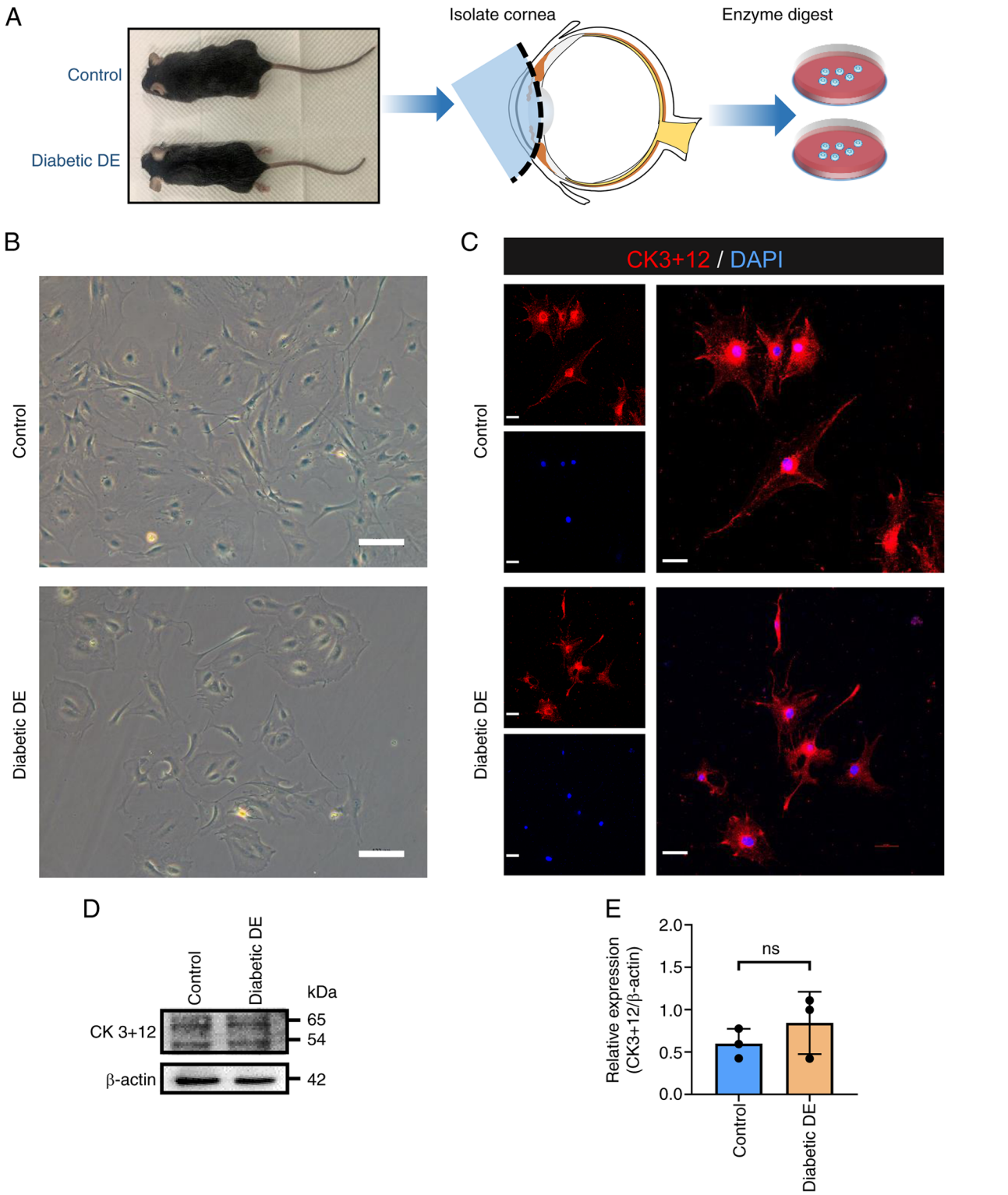


Figure 3. Isolation, culture and identification of primary MCECs in the control and diabetic DE groups. (A) Flow chart of the isolation and culture of primary MCECs by enzymatic digestion in the control and diabetic DE groups. (B) Morphology of primary MCECs in the two groups cultured on days 10 by enzymatic digestion. Scale bar, 100 $\mu$m. (C) Representative IF images demonstrating the distribution of CK3+12 in primary MCECs from the two groups. Scale bar: 100 $\mu$m. (D) Western blot analysis showed CK3+12 protein expression in primary MCECs from the two groups. (E) Densitometry analysis of the data in (D). In (E), data are shown as mean ± standard deviation from three independent experiments. ns, not significant as calculated by two-tailed Student's t-test. MCECs, mouse corneal epithelial cells; DE, dry eye; IF, immunofluorescence.

and resembled spindles, ovals and polygons. The cells in the control group grew rapidly, but those in the diabetic DE group grew slowly and were sparse. This result indicated the poor proliferation of cells in the diabetic DE group.

The cells were subjected to IF staining for CK3+12, a marker of corneal epithelial cells. The CK3+12 protein distributions in the two groups were similar, as illustrated in Fig. 3C. The CK3+12 protein levels in the cells from the two

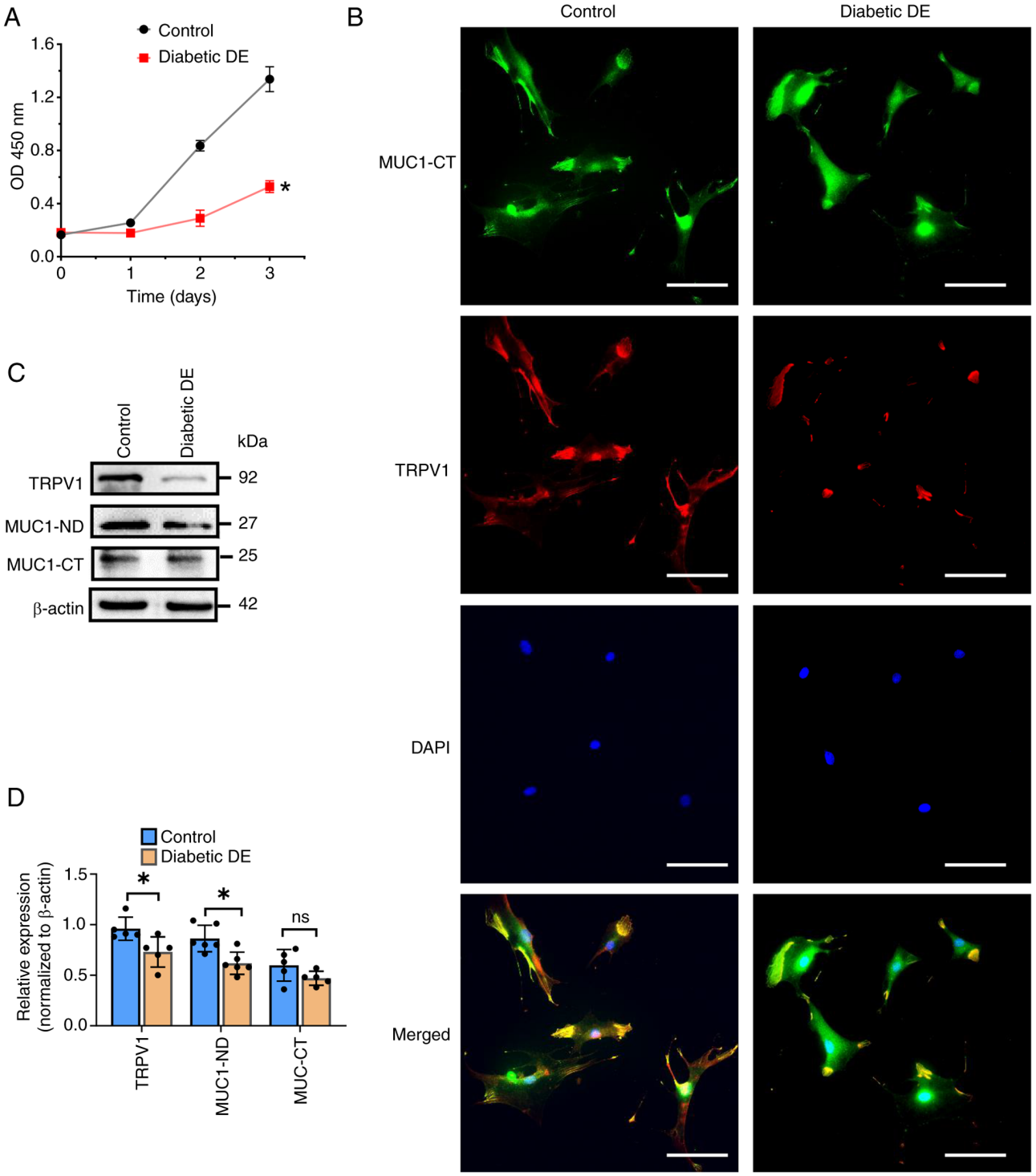


Figure 4. Hyperglycemia impairs cell proliferation, accompanied by decreased MUC1-ND and TRPV1 levels. (A) CCK8 assays showed the cell proliferative ability of the two groups. The OD value at 450 nm was recorded. (B) IF staining was used to locate and detect the expression of MUC1-CT and TRPV1 in primary MCECs from the control and diabetic DE groups. Scale bar, 100 $\mu$m. (C) Western blot analysis of TRPV1, MUC1-ND and MUC1-CT in primary MCECs. β-Actin was used as a loading control. (D) Densitometry analysis of the data in (C). In (A) and (D), data are shown as mean ± standard deviation from three or more independent experiments. ns, not significant, $^{*}$P<0.05 vs. the corresponding control, as analyzed by two-tailed Student's t test. MUC1-ND, MUC1 extracellular domain; TRPV1, transient receptor potential cation channel subfamily V member 1; IF, immunofluorescence; MCECs, mouse corneal epithelial cells; DE, dry eye; MUC1-CT, cytoplasmic tail of MUC1; MUC1, mucin1.

groups were did not significantly differ (Fig. 3D and E). These results identified the cultured cells as corneal epithelial cells.

*Hyperglycemia impairs cell proliferation, accompanied by decreased MUC1-ND and TRPV1.* To further elucidate the functional changes in primary MCECs, CCK8 assays were conducted, which demonstrated attenuated cell proliferation in the diabetic DE group (Fig. 4A). The expression of MUC1-CT and TRPV1 in primary MCECs of the control and diabetic DE groups was detected and the protein localization was assessed

by IF staining (Fig. 4B). The difference in TRPV1 expression between cells in the control and diabetic DE groups was visible, but a difference in MUC1-CT expression was not. The colocalization of MUC1-CT and TRPV1 was also observed in the membrane and cytoplasm. In addition, it was observed that TRPV1 and MUC1-ND were significantly downregulated at the protein level in cells of the diabetic DE group by western blotting and densitometry analysis (Fig. 4C and D). However, the MUC1-CT protein levels of the two groups of cells did not significantly differ.

These results indicated that hyperglycemia impaired cell proliferation in the diabetic DE mice, accompanied by reduced MUC1-ND and TRPV1 levels and that TRPV1 and MUC1 may interact in primary MCECs.

*MUC1-ND binds TRPV1 to positively regulate the proliferation of MCECs MUC1-ND interacts with TRPV1.* To further validate the interaction between MUC1-ND and TRPV1, IF colocalization analysis of frozen corneal sections from the two groups and Co-IP analysis of the two groups of cells were conducted. The distribution and expression of TRPV1 and MUC1-ND are shown in Fig. 5A. IF staining confirmed that TRPV1 and MUC1-ND colocalized in the cell membrane and cytoplasm of the corneal epithelium. The present study also observed reduced TRPV1 and MUC1-ND expression in corneal tissues from the diabetic DE mice in comparison with the control mice. IF colocalization analysis of IF staining images were conducted by ImageJ software to obtain Pearson's correlation coefficients, which were used for statistical analysis. As illustrated in Fig. 5B and C, the Pearson r between MUC1-ND and TRPV1 in the diabetic DE group was 0.60±0.12, which was significantly lower than that in the control group (0.82±0.13). This result indicated that the colocalization of MUC1-ND and TRPV1 was reduced in the diabetic DE mice. Additionally, Co-IP analysis of the two groups of cells was carried out and the association of TRPV1 and MUC1-ND was observed (Fig. 5D). The present study found evidence that MUC1-ND interacted with TRPV1 in the control cells. By contrast, TRPV1 did not coimmunoprecipitate with MUC1-ND in the diabetic DE cells. The present study also tried IP:TRPV1 to immunoblot mucin1-CT and mucin1-ND to immunoblot TRPV1 (Fig. S1), it found that TRPV1 did not interact with mucin1-CT in the control or diabetic DE cells, which may be related to the binding site between the two proteins. These results illustrated that the interaction between MUC1-ND and TRPV1 in the corneal epithelium was decreased in the diabetic DE mice, which may be related to the downregulation of MUC1-ND and TRPV1 in the diabetic DE mice.

*TRPV1 positively regulates cell proliferation.* To verify the regulatory role of TRPV1 in cell proliferation, primary MCECs of the control and diabetic DE groups were treated with CPZ (0, 10 and 30 $\mu$M), a TRPV1 antagonist. Cell viability was detected by CCK8 assays, as shown in Fig. 5E. The viability in control group cells treated with CPZ at 30 $\mu$M was significantly lower than that of cells treated without CPZ treatment ($P<0.01$) and cells treated with CPZ at 10 $\mu$M ($P<0.05$). However, there was no significant difference in cell viability between the untreated cells and cells treated with 10 $\mu$M CPZ. In the diabetic DE group, the lowest cell viability was found in cells treated with CPZ at 30 $\mu$M, followed by those treated with CPZ at 10 $\mu$M and those without CPZ treatment. The viability of cells treated with 10 $\mu$M CPZ and 30 $\mu$M CPZ was significantly lower than that of cells without CPZ treatment ($P<0.001$, $P<0.001$). However, the cell viability of cells treated with 10 $\mu$M CPZ was similar to that of cell treated with 30 $\mu$M CPZ. Collectively, these results demonstrated that CPZ, a TRPV1 antagonist, restricted cell proliferation as its concentration increased.

These data suggested that MUC1-ND interacts with TRPV1, which can positively regulate cell proliferation.

*TRPV1 promotes cell proliferation by partly activating the AKT signaling pathway.* To clarify the mechanism by which the binding of MUC1-ND and TRTV1 regulates cell proliferation, western blotting and CCK8 assays were conducted. Primary MCECs in the control and diabetic DE groups were treated with CPZ (0, 10 and 30 $\mu$M) for 24 h and then harvested for western blotting. CPZ was formulated with DMSO as a solvent, so CPZ 0 $\mu$M meant cells treated with DMSO in the control or diabetic DE groups. As shown in Fig. 6A, there was decreased expression of TRPV1 in control cells treated with CPZ at 30 $\mu$M and diabetic DE cells treated with CPZ at 0, 10 and 30 $\mu$M, indicating that TRPV1 expression was inhibited by CPZ. As shown in Fig. 6A and B, similar levels of AKT1/2/3 in the control groups were observed but in diabetic DE groups, it was significantly increased in 30 $\mu$M CPZ group compared with 0 $\mu$M CPZ group. The level in the diabetic DE + 10 $\mu$M CPZ group was similar to the other two diabetic DE groups. The expression of p-AKT(Ser473) decreased significantly with CPZ treatment in a dose-dependent manner in the control groups and the lowest level was observed in the diabetic DE + 30 $\mu$M CPZ group (Fig. 6A and C). The expression in diabetic DE + 10 $\mu$M CPZ group was not significantly different from the other two diabetic DE groups. The expression of Bcl2 decreased with CPZ treatment in a dose-dependent manner in the control and diabetic DE groups. The protein level of caspase3 increased in diabetic DE groups compared with the control groups with different CPZ treatment. It was more abundant in the control + 30 $\mu$M CPZ group than in control groups treated with 0 and 10 $\mu$M CPZ. Similar levels was found in the three diabetic DE groups. These results suggested that CPZ, a TRPV1 antagonist, attenuated the AKT signaling pathway.

In addition, western blotting was performed to detect the protein expression of AKT1/2/3, p-AKT (Ser473), p-AKT (Thr308), caspase3 and Bcl2. As illustrated in Fig. 6D and E, the protein levels of p-AKT (Ser473) and Bcl2 were significantly reduced in the diabetic DE group, but the protein levels of AKT1/2/3, p-AKT (Thr308) and caspase3 was significantly increased in the diabetic DE group when compared with the control group. The results indicated that activation of the AKT signaling pathway was attenuated in the diabetic DE mice.

Furthermore, cells in the control group were treated with DMSO, 30 $\mu$M CPZ or treated with 30 $\mu$M CPZ + 1 $\mu$M MK2206 (an AKT inhibitor) for 24 h. Then, CCK8 assays were conducted to detect cell viability and western blotting. As shown in Fig. 6F, the cell viability of the 30 $\mu$M CPZ-treated group was significantly lower than that of the untreated group

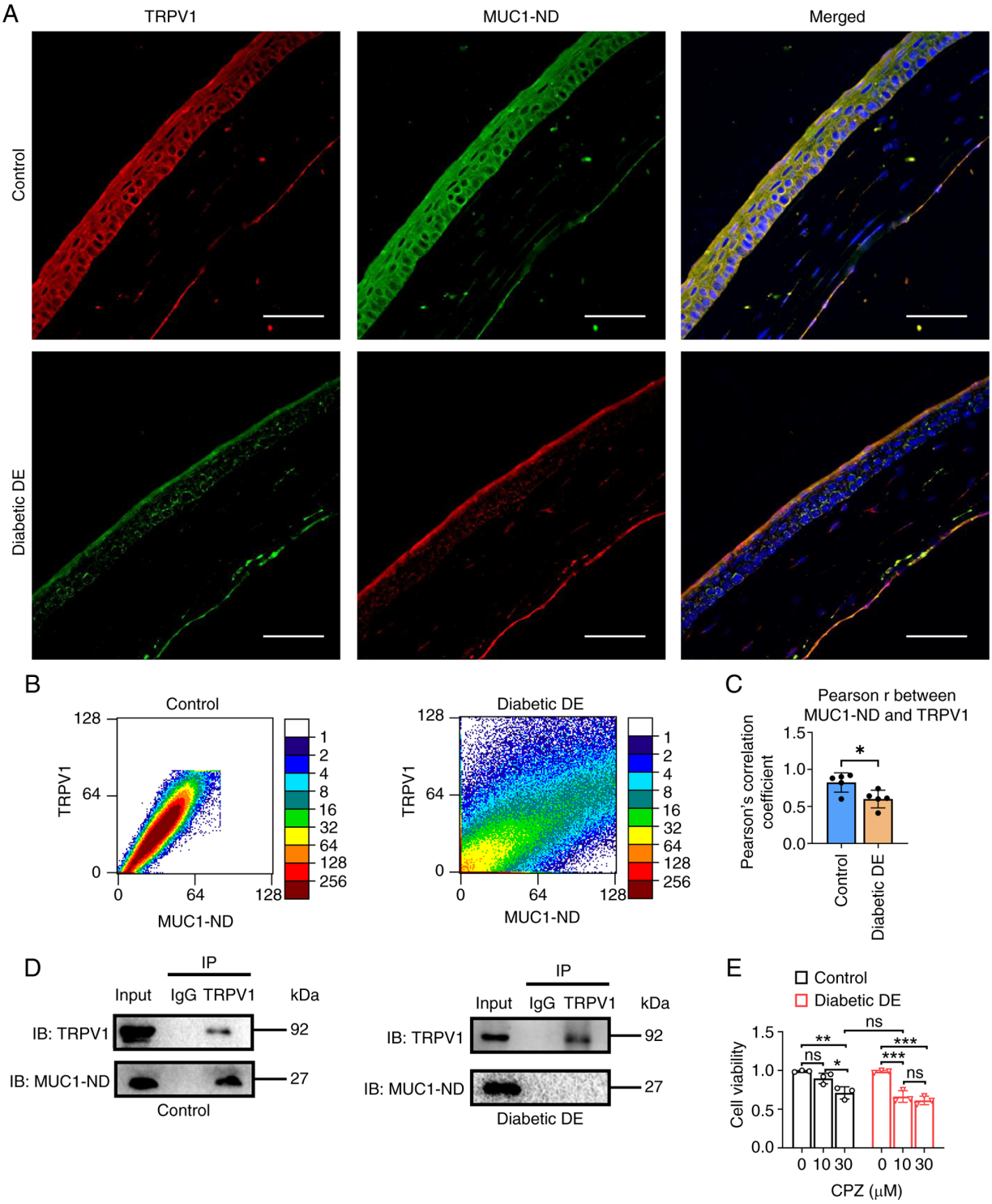


Figure 5. TRPV1 interacts with MUC1-ND to promote cell viability. (A) Frozen corneal sections were stained for TRPV1 and MUC1-ND in the control and diabetic DE groups. Three channels (red, blue and green, right panel) were used for IF analysis. n=5 animals per group. Scale bar, 50 $\mu$m. (B) Scatter diagram from IF colocalization analysis of the data in (A) by ImageJ software. (C) Statistical analysis of the Pearson r between TRPV1 and MUC1-ND in the corneal epithelium in the two groups. n=5 animals per group. (D) Coimmunoprecipitation and western blotting showed that TRPV1 bound MUC1-ND in primary MCECs from the two groups. (E) CCK8 assays detected the cell viability of the two groups after treatment with CPZ (0, 10 and 30 $\mu$M), a TRPV1 antagonist. In (C) and (E), data are shown as mean ± standard deviation from at least three independent experiments. ns: not significant, $^{*}$P<0.05, $^{**}$P<0.01, $^{***}$P<0.001 vs. the corresponding control, as analyzed by either two-tailed Student's t test for two groups or by one-way ANOVA with LSD's multiple-comparison test for more than two groups. TRPV1, transient receptor potential cation channel subfamily V member 1; MUC1-ND, MUC1 extracellular domain; MUC1, mucin1; DE, dry eye; IF, immunofluorescence; MCECs, mouse corneal epithelial cells; CPZ, capsazepine.

but was not significantly different from that of the CPZ + MK2206-treated group. The cell viability of the CPZ + MK2206-treated group was significantly lower than that of the DMSO group (P<0.001). These results demonstrated that AKT signaling pathway inhibition was partly responsible for the effect of CPZ (a TRPV1 antagonist) on cell proliferation. As

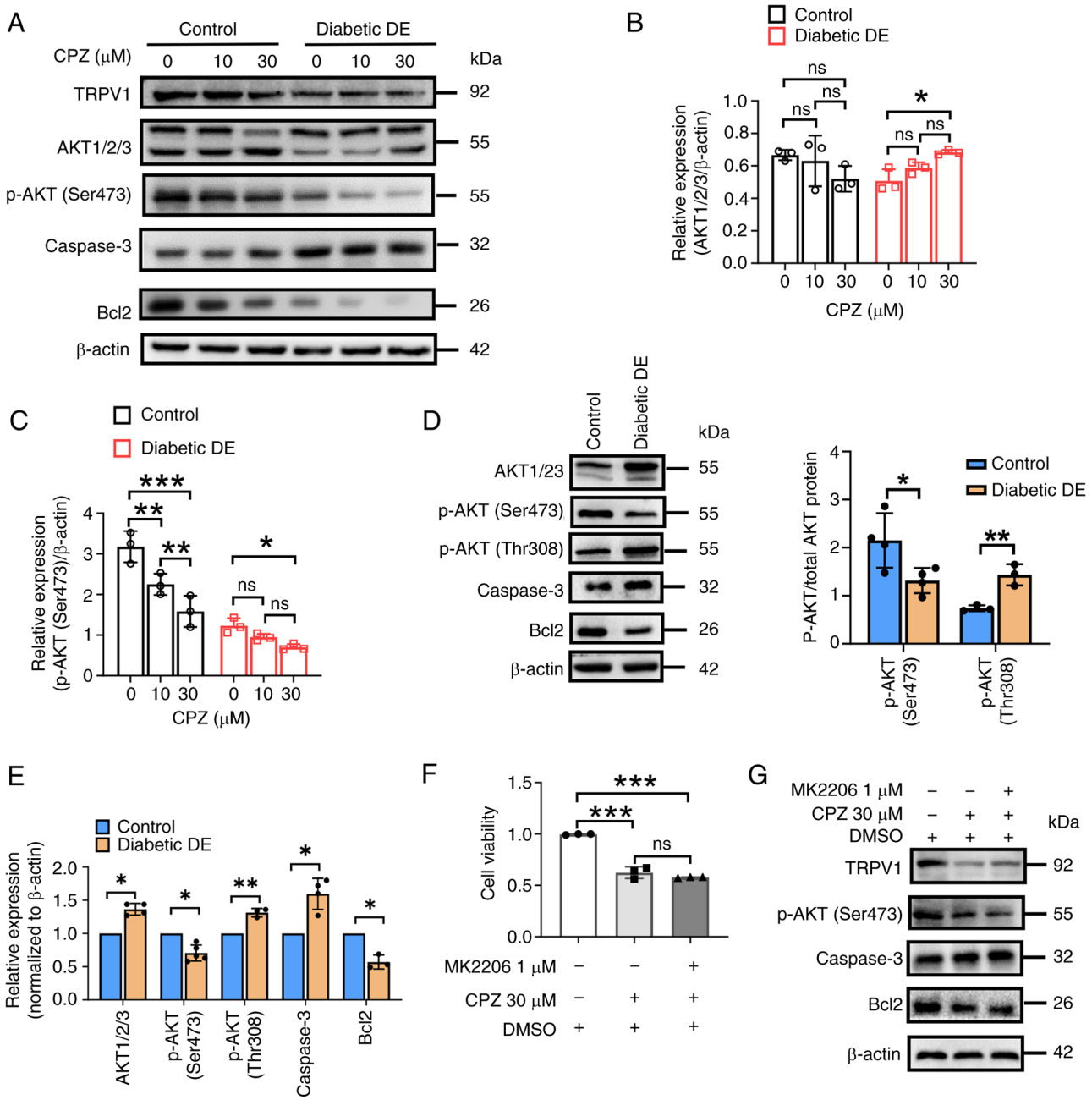


Figure 6. TRPV1 positively regulates cell proliferation by partly activating the AKT pathway. (A) Western blotting showing the protein expression of TRPV1, AKT1/2/3, p-AKT (Ser473), p-AKT (Thr308), caspase3 and Bcl2 in the two groups of cells upon treatment with the TRPV1 antagonist CPZ (0, 10 and 30 $\mu$M) for 24 h. (B and C) Densitometry analysis of AKT1/2/3, p-AKT (Ser473) in (A). (D) Western blotting and (E) densitometry analysis of the protein expression of AKT1/2/3, p-AKT (Ser473), p-AKT (Thr308), caspase3 and Bcl2 in primary MCECs of the control and diabetic DE groups. (F) CCK8 assays showed the cell viability in the control group without CPZ treatment and upon treatment with CPZ at 30 $\mu$M or with CPZ at 30 $\mu$M + MK2206 (an AKT inhibitor) at 1 $\mu$M for 24 h. Western blotting showing the protein expression of TRPV1, p-AKT (Ser473), caspase3 and Bcl2 in primary MCECs of the diabetic DE group treated as described in (G). In (B, C and F), quantified data are shown as mean ± standard deviation from three or more independent experiments. ns, not significant, $^{*}$P<0.05, $^{**}$P<0.01, $^{***}$P<0.001 vs. the corresponding control, by either two-tailed Student's t-test for two groups or by one-way ANOVA followed by LSD multiple-comparison test for more than two groups. TRPV1, transient receptor potential cation channel subfamily V member 1; p-, phosphorylated; CPZ, capsazepine; DE, dry eye; STZ, streptozotocin.

shown in Fig. 6G, the protein expressions of TRPV1, p-AKT (Ser473) and Bcl2 were reduced in other two groups compared with that of the DMSO group. The caspase3 protein level was increased in the 30 $\mu$M CPZ-treated group and the CPZ + MK2206-treated group.

The aforementioned results suggested that TRPV1 positively regulated cell proliferation by partly activating the AKT signaling pathway.

## Discussion

The present study investigated the biological role of the MUC1-ND/TRPV1/AKT axis in the moderation of corneal epithelial cells in diabetic mice with DE disease. First, diabetic DE model mice were established with significantly increased corneal epithelial defects, reduced tear production, poor TF pattern grades and an impaired ocular surface structure.

Second, the expression levels of MUC1-ND and TRPV1 were found to be significantly reduced in the corneal epithelium of diabetic DE mice. Third, TRPV1 was shown to positively regulate the proliferation of MCECs. Notably, MUC1-ND was shown to interact with the TRPV1 protein in the control group but not in the diabetic DE group. Furthermore, it was found that TRPV1 positively regulated cell proliferation by partly activating the AKT signaling pathway. In general, the present study revealed that the interaction between MUC1-ND and TRPV1 partly activated the AKT signaling pathway to promote MCEC proliferation.

DE disease is a multifactorial disorder and its most distinguished feature is the loss of homeostasis of the tear film (2). The establishment of DE animal models is necessary to study the fundamental mechanisms of DE disease, which is nearly identical in animals and in humans (34). Previous studies have confirmed that DE animal models, including chemical- or surgery-induced DE models, environmental factor-induced DE models, genetically engineered DE models and models prepared with combined methods, are reliable and effective in imitating ocular surface microenvironments (34,35). Common parameters used to evaluate DE disease in mouse models are CFS to assess surface structure, the TF test to assess tear proteins, the phenol red thread test to assess tear secretion and histopathological examination (34,35). In the present study, the diabetic mice were followed for 60 days and it was confirmed that they exhibited significantly increased corneal epithelial defects, decreased tear production, poor TF pattern grades, impaired corneal epithelial structure and a lower goblet cell density on day 30 following the final STZ injection. The method used to establish the diabetic DE model was similar to that used in another previous study (36). The diabetic DE model mice were identified to be reliable tools in the study of pathophysiological mechanisms and the underlying molecular cascade in diabetic DE disease. Notably, it was also observed that TF was lessened and even disappeared in diabetic mice with DE, indicating that the tear proteins differed in diabetic mice with DE disease. Then, primary MCECs from mice in the control and diabetic DE groups were cultured and identified, consistent with a previous study (37).

MUC1 is a key member of the membrane-associated mucin (MAM) family with an important barrier function (15). MUC1 accumulates with other MAMs on the corneal epithelia and it is cross-linked by galectin-3 to form an interlocking lattice for pathogen exclusion (14). Damage to the ocular surface epithelium and barrier disruption causes ocular surface diseases, including DE disease. One clinical study reported that MUC1 expression levels were decreased in the conjunctival epithelium of patients with DE disease (38). MUC1 is also confirmed to be cleaved at its extracellular domain (MUC1-ND) (19,20). Part of the soluble extracellular subunit of MUC1 can be detected in human tears (39). In the present study, MUC1-CT expression was found decreased in diabetic DE mice, but the difference was not significant compared with that of the control mice, whereas MUC1-ND levels were significantly decreased in the corneal epithelial cells of diabetic DE mice compared with control mice. This suggested that MUC1 was cleaved and that its soluble extracellular large subunit (MUC1-ND) was shed from the corneal epithelial cell surface in diabetic mice with DE disease. The present study revealed that MUC1 abnormalities may be closely linked with corneal epithelial homeostasis in diabetic DE disease.

Growing evidence shows the downregulation of TRPV1 in colorectal, endometrial, renal and skin cancers but the upregulation of TRPV1 in the U373 glioblastoma line, high-grade astrocytes and the RT4 renal cell carcinoma line, indicating that TRPV1 mediates the balance between cell proliferation and apoptosis (40). TRPV1 activation acts as a double-edged sword in that it induces both improvements in cell proliferation and migration in corneal injury (41-43) and the release of proinflammatory cytokines in human corneal epithelial cells stimulated by hyperosmolarity (25,44,45). Previous studies (30,31,46) have also shown that MUC1 regulates inflammation via interactions with several different signaling pathways and correlates with the stabilization of ion channels, which are essential to corneal epithelial homeostasis (15). MUC1 forms a lattice with TRPV5 via galectin-3 to increase renal TRPV5 activity to protect against nephrolithiasis (30). The present study first confirmed the downregulation of TRPV1 in the corneal epithelia of diabetic DE mice compared with control mice. It next analyzed the relationship between TRPV1 levels and corneal cell proliferation. It was found that CPZ, a TRPV1 antagonist, restricted proliferation in primary MCECs, indicating that TRPV1 played a key role in promoting MCEC proliferation in diabetic DE disease. The present study further investigated the interaction between MUC1 and TRPV1 and the results demonstrated that MUC1-ND interacted with the TRPV1 protein in the control group but not in the diabetic DE group. These results demonstrated that the interaction between MUC1-ND and TRPV1 positively promoted corneal epithelial cell proliferation. This interaction was attenuated in the diabetic mice and may contribute to corneal epithelial dysfunction in DE disease.

The Ser and Thr kinase AKT, also known as protein kinase B (PKB), has become the focus in biological and medicinal studies, together with its function and regulation in diabetes (47). AKT activation occurs downstream of inositol phosphate 3-kinase (PI3K), a lipid kinase associated with cell transformation and the insulin response. The activation of PI3K leads to the phosphorylation of two key residues on AKT1, catalyzing the activation of Thr308 in the T loop and Ser473 in the C-terminal hydrophobic motif. AKT activation is greatly decreased when Ser473 is unphosphorylated, which stabilizes Thr308 phosphorylation and AKT activation. Attenuated activation of the AKT signaling pathway inhibits corneal epithelial wound healing in a model of corneal epithelial trauma in diabetic mice (48). Some studies have found that TRPV1 channel activation can result in the phosphorylation of AKT for signal transduction (29,49). The present study found that the AKT signaling pathway was attenuated in diabetic mice with DE disease, accompanied by the decreased phosphorylation of AKT (Ser473). Additionally, it was found that CPZ, a TRPV1 antagonist, reduced the activation of the AKT signaling pathway. However, this inhibition was partly responsible for the effect of CPZ (a TRPV1 antagonist) on cell proliferation. Collectively, these findings revealed that TRPV1 positively regulated cell proliferation by partly activating the AKT signaling pathway. Notably, the present study revealed the interaction between MUC1-ND and TRPV1 and its regulation in the corneal epithelial cells of diabetic DE mice. In the

present study it was found that MUC1-ND acts as a protein partner that interacts with TRPV1, which positively regulates MCEC proliferation by partly activating the AKT signaling pathway. The decrease in this interaction in the diabetic mice may have induced corneal epithelial dysfunction in the progression of diabetic DE disease.

There was limitation to the present study. MUC1-ND in the tears of diabetic mice failed to be detected via western blotting, due to very little tear secretion from the mice. It may be an improvement to collect the tear fluid of diabetic patients with dry eye disease to detect the mucin1-ND level. Relevant clinical trials are required to assess the role of MUC1-ND and TRPV1 in diabetic DE disease.

In summary, the present study illustrated that the interaction of MUC1-ND with TRPV1 promoted MCEC proliferation by partly activating the AKT signaling pathway. The findings provided new insight into the pathogenesis of corneal epithelial dysfunction in diabetic DE disease.

**Acknowledgements**

Not applicable.

**Funding**

The present study was supported by Natural Science Foundation of Guangdong Province, China (project no. 2022A1515012346) and the Science and Technology Program of Guangzhou, China (project no. 202002020046).

**Availability of data and materials**

The data generated in the present study may be requested from the corresponding author.

**Authors' contributions**

HQL, XHL, YZ and YYZ contributed to the study design. HQL, YZ, YTC, RZ, XHL, YYZ, WKZ, HC, JH and SFF conducted experiments. HQL and YZ performed statistical analysis and drafted the manuscript. HQL and YZ confirm the authenticity of all the raw data. All authors read and approved the final manuscript.

**Ethics approval and consent to participate**

All experimental procedures were approved by the Institutional Animal Care and Use Committee of Southern Medical University (Guangzhou, China; approval no. LAEC-2021-032) and conducted in compliance with the ARVO statement for the Use of Animals in Ophthalmic and Vision Research (32).

**Patient consent for publication**

Not applicable.

**Competing interests**

The authors declare that they have no competing interests.

**References**

1. Ogurtsova K, Guariguata L, Barengo NC, Ruiz PL, Sacre JW, Karuranga S, Sun H, Boyko EJ and Magliano DJ: IDF diabetes Atlas: Global estimates of undiagnosed diabetes in adults for 2021. Diabetes Res Clin Pract 183: 109118, 2022.
2. Craig JP, Nichols KK, Akpek EK, Caffery B, Dua HS, Joo CK, Liu Z, Nelson JD, Nichols JJ, Tsubota K and Stapleton F: TFOS DEWS II definition and classification report. Ocul Surf 15: 276-283, 2017.
3. Stapleton F, Alves M, Bunya VY, Jalbert I, Lekhanont K, Malet F, Na KS, Schaumberg D, Uchino M, Vehof J, *et al*: TFOS DEWS II epidemiology report. Ocul Surf 15: 334-365, 2017.
4. Manaviat MR, Rashidi M, Afkhami-Ardekani M and Shoja MR: Prevalence of dry eye syndrome and diabetic retinopathy in type 2 diabetic patients. BMC Ophthalmol 8: 10, 2008.
5. Zhang X, Zhao L, Deng S, Sun X and Wang N: Dry eye syndrome in patients with diabetes mellitus: Prevalence, etiology, and clinical characteristics. J Ophthalmol 2016: 8201053, 2016.
6. Belmonte C, Nichols JJ, Cox SM, Brock JA, Begley CG, Bereiter DA, Dartt DA, Galor A, Hamrah P, Ivanusic JJ, *et al*: TFOS DEWS II pain and sensation report. Ocul Surf 15: 404-437, 2017.
7. Shih KC, Lam KS and Tong L: A systematic review on the impact of diabetes mellitus on the ocular surface. Nutr Diabetes 7: e251, 2017.
8. Han SB, Yang HK and Hyon JY: Influence of diabetes mellitus on anterior segment of the eye. Clin Interv Aging 14: 53-63, 2018.
9. Kaiserman I, Kaiserman N, Nakar S and Vinker S: Dry eye in diabetic patients. Am J Ophthalmol 139: 498-503, 2005.
10. Zhu L, Titone R and Robertson DM: The impact of hyperglycemia on the corneal epithelium: Molecular mechanisms and insight. Ocul Surf 17: 644-654, 2019.
11. Georgiev GA, Eftimov P and Yokoi N: Contribution of mucins towards the physical properties of the tear film: A modern update. Int J Mol Sci 20: 6132, 2019.
12. Ablamowicz AF and Nichols JJ: Ocular surface membrane-associated mucins. Ocul Surf 14: 331-341, 2016.
13. Shirai K and Saika S: Ocular surface mucins and local inflammation-studies in genetically modified mouse lines. BMC Ophthalmol 15 (Suppl 1): S154, 2015.
14. Martinez-Carrasco R, Argüeso P and Fini ME: Membrane-associated mucins of the human ocular surface in health and disease. Ocul Surf 21: 313-330, 2021.
15. Fini ME, Jeong S, Gong H, Martinez-Carrasco R, Laver NMV, Hijikata M, Keicho N and Argüeso P: Membrane-associated mucins of the ocular surface: New genes, new protein functions and new biological roles in human and mouse. Prog Retin Eye Res 75: 100777, 2020.
16. Schroeder JA, Thompson MC, Gardner MM and Gendler SJ: Transgenic MUC1 interacts with epidermal growth factor receptor and correlates with mitogen-activated protein kinase activation in the mouse mammary gland. J Biol Chem 276: 13057-13064, 2001.
17. Li Y, Ren J, Yu W, Li Q, Kuwahara H, Yin L, Carraway KL III and Kufe D: The epidermal growth factor receptor regulates interaction of the human DF3/MUC1 carcinoma antigen with c-Src and beta-catenin. J Biol Chem 276: 35239-35242, 2001.
18. Morimoto Y, Yamashita N, Daimon T, Hirose H, Yamano S, Haratake N, Ishikawa S, Bhattacharya A, Fushimi A, Ahmad R, *et al*: MUC1-C is a master regulator of MICA/B NKG2D ligand and exosome secretion in human cancer cells. J Immunother Cancer 11: e006238, 2023.
19. Thathiah A, Blobel CP and Carson DD: Tumor Necrosis Factor-alpha Converting Enzyme/ADAM 17 Mediates MUC1 Shedding. J Biol Chem 278: 3386-3394, 2003.
20. Thathiah A and Carson DD: MT1-MMP mediates MUC1 shedding independent of TACE/ADAM17. Biochem J 382 (Pt 1): 363-373, 2004.
21. Miyazaki K, Kishimoto H, Kobayashi H, Suzuki A, Higuchi K, Shirasaka Y and Inoue K: The glycosylated N-terminal domain of MUC1 is involved in chemoresistance by modulating drug permeation across the plasma membrane. Mol Pharmacol 103: 166-175, 2023.
22. Liu R, Chen L, Zhao X, Bao L, Wei R and Wu X: MUC1 promotes RIF by regulating macrophage ROS-SHP2 signaling pathway to up-regulate inflammatory response and inhibit angiogenesis. Aging (Albany NY) 16: 3790-3802, 2024.

23. Liu L, Zhou L, Wang L, Mao Z, Zheng P, Zhang F, Zhang H and Liu H: MUC1 attenuates neutrophilic airway inflammation in asthma by reducing NLRP3 inflammasome-mediated pyroptosis through the inhibition of the TLR4/MyD88/NF-κB pathway. Respir Res 24: 255, 2023.
24. Comes N, Gasull X and Callejo G: Proton sensing on the ocular surface: Implications in eye pain. Front Pharmacol 12: 773871, 2021.
25. Yang Y, Yang H, Wang Z, Okada Y, Saika S and Reinach PS: Wakayama symposium: Dependence of corneal epithelial homeostasis on transient receptor potential function. Ocul Surf 11: 8-11, 2013.
26. Yang XL, Wang X, Shao L, Jiang GT, Min JW, Mei XY, He XH, Liu WH, Huang WX and Peng BW: TRPV1 mediates astrocyte activation and interleukin-1β release induced by hypoxic ischemia (HI). J Neuroinflammation 16: 114, 2019.
27. Wang X, Yang XL, Kong WL, Zeng ML, Shao L, Jiang GT, Cheng JJ, Kong S, He XH, Liu WH, *et al*: TRPV1 translocated to astrocytic membrane to promote migration and inflammatory infiltration thus promotes epilepsy after hypoxic ischemia in immature brain. J Neuroinflammation 16: 214, 2019.
28. Lu MJ, Chen YS, Huang HS and Ma MC: Hypoxic preconditioning protects rat hearts against ischemia-reperfusion injury via the arachidonate12-lipoxygenase/transient receptor potential vanilloid 1 pathway. Basic Res Cardiol 109: 414, 2014.
29. Yang H, Wang Z, Capó-Aponte JE, Zhang F, Pan Z and Reinach PS: Epidermal growth factor receptor transactivation by the cannabinoid receptor (CB1) and transient receptor potential vanilloid 1 (TRPV1) induces differential responses in corneal epithelial cells. Exp Eye Res 91: 462-471, 2010.
30. Nie M, Bal MS, Yang Z, Liu J, Rivera C, Wenzel A, Beck BB, Sakhaee K, Marciano DK and Wolf MT: Mucin-1 Increases Renal TRPV5 activity in vitro, and urinary level associates with calcium nephrolithiasis in patients. J Am Soc Nephrol 27: 3447-3458, 2016.
31. Al-Bataineh MM, Kinlough CL, Marciszyn A, Lam T, Ye L, Kidd K, Maggiore JC, Poland PA, Kmoch S, Bleyer A, *et al*: Influence of glycoprotein MUC1 on trafficking of the Ca2+-selective ion channels, TRPV5 and TRPV6, and on in vivo calcium homeostasis. J Biol Chem 299: 102925, 2023.
32. The Association for Research in Vision and Ophthalmology: ARVO Statement for the Use of Animals in Ophthalmic and Vision Research. The Association for Research in Vision and Ophthalmology, Rockville, MD, 2021.
33. Masmali AM, Murphy PJ and Purslow C: Development of a new grading scale for tear ferning. Cont Lens Anterior Eye 37: 178-184, 2014.
34. Rahman MM, Kim DH, Park CK and Kim YH: Experimental models, induction protocols, and measured parameters in dry eye disease: Focusing on practical implications for experimental research. Int J Mol Sci 22: 12102, 2021.
35. Zhu J, Inomata T, Shih KC, Okumura Y, Fujio K, Huang T, Nagino K, Akasaki Y, Fujimoto K, Yanagawa A, *et al*: Application of animal models in interpreting dry eye disease. Front Med (Lausanne) 9: 830592, 2022.
36. Qu M, Wan L, Dong M, Wang Y, Xie L and Zhou Q: Hyperglycemia-induced severe mitochondrial bioenergetic deficit of lacrimal gland contributes to the early onset of dry eye in diabetic mice. Free Radic Biol Med 166: 313-323, 2021.
37. Bai J, Fu H, Bazinet L, Birsner AE and D'Amato RJ: A method for developing novel 3D Cornea-on-a-Chip using primary murine corneal epithelial and endothelial cells. Front Pharmacol 11: 453, 2020.
38. Corrales RM, Narayanan S, Fernández I, Mayo A, Galarreta DJ, Fuentes-Páez G, Chaves FJ, Herreras JM and Calonge M: Ocular mucin gene expression levels as biomarkers for the diagnosis of dry eye syndrome. Invest Ophthalmol Vis Sci 52: 8363-8369, 2011.
39. Spurr-Michaud S, Argüeso P and Gipson I: Assay of mucins in human tear fluid. Exp Eye Res 84: 939-950, 2007.
40. Zhai K, Liskova A, Kubatka P and Büsselberg D: Calcium Entry through TRPV1: A potential target for the regulation of proliferation and apoptosis in cancerous and healthy cells. Int J Mol Sci 21: 4177, 2020.
41. Sumioka T, Okada Y, Reinach PS, Shirai K, Miyajima M, Yamanaka O and Saika S: Impairment of corneal epithelial wound healing in a TRPV1-deficient mouse. Invest Ophthalmol Vis Sci 55: 3295-3302, 2014.
42. Okada Y, Reinach PS, Shirai K, Kitano A, Kao WW, Flanders KC, Miyajima M, Liu H, Zhang J and Saika S: TRPV1 involvement in inflammatory tissue fibrosis in mice. Am J Pathol 178: 2654-2664, 2011.
43. Nidegawa-Saitoh Y, Sumioka T, Okada Y, Reinach PS, Flanders KC, Liu CY, Yamanaka O, Kao WW and Saika S: Impaired healing of cornea incision injury in a TRPV1-deficient mouse. Cell Tissue Res 374: 329-338, 2018.
44. Pan Z, Wang Z, Yang H, Zhang F and Reinach PS: TRPV1 activation is required for hypertonicity-stimulated inflammatory cytokine release in human corneal epithelial cells. Invest Ophthalmol Vis Sci 52: 485-493, 2011.
45. Reinach PS, Mergler S, Okada Y and Saika S: Ocular transient receptor potential channel function in health and disease. BMC Ophthalmol 15 (Suppl 1): S153, 2015.
46. Jeon BH, Yoo YM, Jung EM and Jeung EB: Dexamethasone treatment increases the intracellular calcium level through TRPV6 in A549 cells. Int J Mol Sci 21: 1050, 2020.
47. Manning BD and Toker A: AKT/PKB Signaling: Navigating the network. Cell 169: 381-405, 2017.
48. Li Y, Li J, Zhao C, Yang L, Qi X, Wang X, Zhou Q and Shi W: Hyperglycemia-reduced NAD+ biosynthesis impairs corneal epithelial wound healing in diabetic mice. Metabolism 114: 154402, 2021.
49. Pham TH, Jin SW, Lee GH, Park JS, Kim JY, Thai TN, Han EH and Jeong HG: Sesamin induces endothelial nitric oxide synthase activation via transient receptor potential vanilloid type 1. J Agric Food Chem 68: 3474-3484, 2020.